

First-principles study of electronic and optical properties of cubic perovskite CsSrF₃

K. EPHRAIM BABU, A. VEERAI AH, D. TIRUPATHI SWAMY, V. VEERAI AH*

Modelling and Simulation in Material Science Laboratory, Department of Physics,
Andhra University, Visakhapatnam, Andhra Pradesh, 530003, India.

We present first principles calculations of the electronic, structural and optical properties of the cubic perovskite CsSrF₃ by using the full potential linearized augmented plane wave (FP-LAPW) plus local orbitals method with generalized gradient approximation (GGA) in the frame work of density functional theory. The calculated lattice constant is in a good agreement with the experimental result. The electronic band structure shows that the fundamental band gap is wide and direct at Γ point. The contribution of the different bands was analyzed from the total and partial density of states curves. The charge density plots show strong ionic bonding in Cs-F, ionic and weak covalent bonding between Sr and F. The calculated optical spectra viz., the dielectric function, optical reflectivity, absorption coefficient, real part of optical conductivity, refractive index, extinction coefficient and electron energy loss, are presented for the energy range of 0-30 eV.

Keywords: *cubic perovskite, FP-LAPW, wide band gap, opto-electronic material.*

© Wrocław University of Technology.

1. Introduction

It is well known that materials with perovskite structures find applications in many areas of science and technology due to their electro-optic, electro-mechanical properties and non-linear properties. In the last decade, many experimental and theoretical investigations have been devoted to the study of perovskite-type fluorides: typically ABF₃ (A: large cation with different valence and B: transition metal). This class of materials has a great potential for a variety of device applications in optical, ferroelectric, antiferromagnetic systems [1–5] due to their wide band gaps. The Cs-based CsXF₃ (X = Ca, Sr, Cd, and Pb) materials are a class of perovskite type fluorides [6]. This family of perovskite fluorides, CsXF₃ shows a larger Cs–F distance than the X–F one. This type of fluoroperovskites shows photo- and thermo-stimulated luminescence properties [7], tunable laser action, electron-phonon interactions, and phase transition behaviors when doped with some transition metal ions [8]. The topological analysis of the electronic structure for CsSrF₃

was investigated by Victor Luana et al. [9]. Metal fluorides have unique optical properties such as low refractive index and they are extensively used in anti-reflection and protective coatings. Structural and optoelectronic properties of cubic CsPbF₃ perovskite was reported by Murtaza et al. [10], and the Authors predicted that CsPbF₃ is suitable for optoelectronic devices and anti-reflecting coating.

The highly ionic nature of the chemical bond in CsSrF₃ ensures the applicability of well developed quantum mechanical models corresponding to the ionic approximations in solids. As CsSrF₃ is a direct band gap compound and is optically active [11], it can be effectively used in photonic and optoelectronic devices. The magnetic shielding constant of ¹³³Cs nuclei in CsSrF₃ was reported as 3.40 Å [12]. Magnetic shielding constants observed by nuclear magnetic resonance (NMR) spectroscopy sensitively reflect the valence electronic structures of molecules. The theoretical investigation of CsSrF₃ has not yet been studied and published by anyone to the best of our knowledge. Hence we present the electronic and optical properties of the cubic perovskite CsSrF₃ for the first time. The lattice constant of CsSrF₃ was reported to be 4.750 Å by Jiang et

*E-mail: v_veeraiah@yahoo.co.in

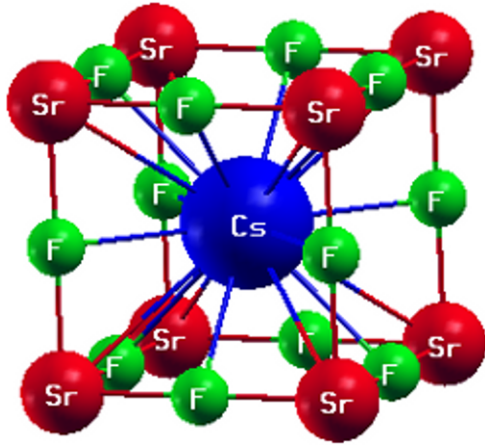


Fig. 1. Structure of cubic perovskite CsSrF₃.

al. [13]. The study of optical properties is aimed at determining the dielectric function, refractive index, absorption coefficient, and energy loss spectroscopy of the CsSrF₃ material. Similar studies of the optoelectronic properties of some materials have been reported in the literature [14–16]. The present study is organized as follows: in Section 2, we briefly describe the computational details used in this work. Results and discussions of our study are presented in Section 3. Finally, conclusions and remarks are given in Section 4.

2. Computational details

Several computational methods have been developed to study the electronic structure of materials based on first principles approaches. They are utilizing the full solution of the ground state of the electronic system within the local-density approximation (LDA) to Kohn-Sham density functional theory (DFT) [17, 18]. Many physical and chemical properties of the condensed matter can be predicted accurately using these first principles methods [19, 20]. The crystal structure of CsSrF₃ is illustrated in Fig. 1. The crystal structure belongs to the space group *pm3m* (221) with Cs at (0.5, 0.5, 0.5), Sr at (0, 0, 0) and F at (0.5, 0, 0) positions and origin is chosen to be at (0, 0, 0) [9]. The lattice parameters are taken to be $a = 4.750 \text{ \AA}$ [13]. The calculations presented in this work are performed using the FP-LAPW+lo method.

The electronic and optical properties are calculated using the ab initio full-potential linearized augmented-plane-wave (FP-LAPW) method with the WIEN2k code [21] in the generalized gradient approximation (GGA) of the Perdew–Burke–Ernzerhof (PBE) exchange–correlation potential [22]. In the FP-LAPW method, the unit cell is divided into two parts: (I) non-overlapping atomic spheres (centred at the atomic sites) and (II) an interstitial region. In this method no shape approximation on either potential or electronic charge density is made. By implementation of this method, which allows the inclusion of local orbitals into the basis, we are improving upon linearization and making possible a consistent treatment of semicore and valence states in one energy window and hence ensuring proper orthogonality. The FP-LAPW method expands the potential in the following form:

$$V(r) = \sum_{lm} V_{lm}(r) Y_{lm}(\hat{r}) \quad (\text{insidesphere}) \quad (1)$$

$$V(r) = \sum_k V_k e^{ikr} \quad (\text{outsidesphere}) \quad (2)$$

where, $Y_{lm}(\hat{r})$ is a linear combination of radial functions times spherical harmonics.

The radii of the atomic muffin-tin (MT) spheres are equal to 2.20 a.u. for Cs, 2.00 a.u. for Sr, and 1.50 a.u. for F. The set of plane waves K_{max} is determined from the condition $R_{\text{MT}} K_{\text{max}} = 7.0$. The cut-off energy, which defines the separation between the core and valency states, is set to -6.0 Ry . The integration over the Brillouin zone is performed by the tetrahedron method, using 35 k-points in the irreducible part of the Brillouin zone (BZ). The convergence criterion (for the total energy) is equal to 0.0001 Ry. The optoelectronic properties of the compound are calculated using a denser mesh of 2300 k-points in the Irreducible Brillouin Zone (IBZ).

3. Results and discussions

3.1. Structural optimization

The total energy per unit cell of CsSrF₃ in the cubic perovskite structure is shown in Fig. 2,

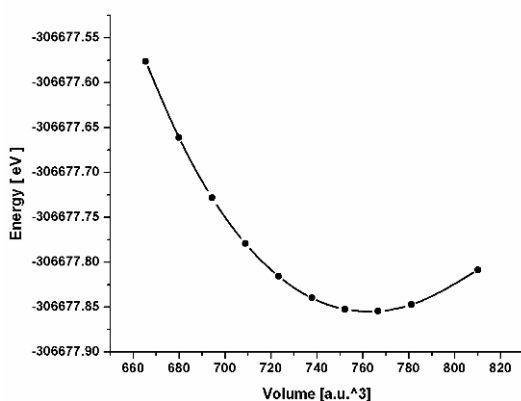


Fig. 2. Dependence of total energy of cubic perovskite CsSrF₃ crystal on unit cell volume.

Table 1. Calculated lattice constant a (Å), bulk modulus B_0 (GPa) and pressure derivative (B').

| Method | Lattice constant a (Å) | B_0 (GPa) | B' |
|--------|--------------------------|-------------|------|
| GGA | 4.83 | 37.7 | 4.86 |
| LDA | 4.64 | 52.4 | 4.83 |
| Expt. | (4.750) ^a | | |

^a Ref. [13], Experimental value

as a function of the lattice constant. The volume versus energy is fitted by the Birch-Murnaghan equation of state [23]. From this fit, we can get the equilibrium lattice constant (a), bulk modulus (B_0) and pressure derivative of the bulk modulus (B'). These values are shown in Table 1. We performed our calculations by using LDA and the GGA approximations. The results show that the calculated equilibrium lattice constant within the LDA is 2.3% lower than the experimental value, while the GGA calculated value is 1.6% larger. The LDA underestimate the lattice constant while the GGA overestimate it. As per the results in the GGA approximation the lattice parameter is closer to the experimental value compared to the LDA approximation. By using LDA approximation the energy minimum is obtained as -306368.5197 eV and with GGA approximation the minimum energy is obtained as -306677.8545 eV. Comparing these two, the GGA approximation energy is minimum. So, we performed the further calculations by using the GGA approximation.

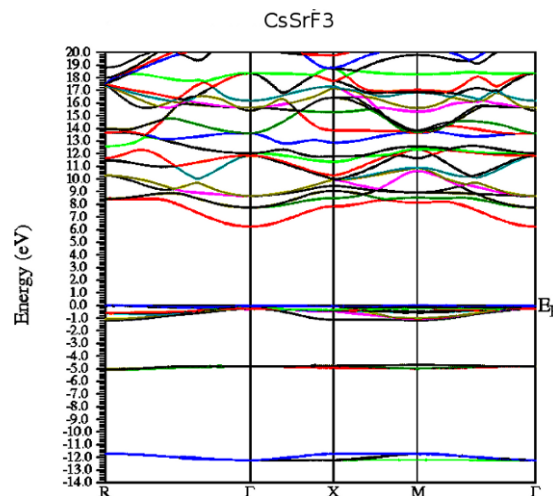


Fig. 3. Calculated band structure of cubic perovskite CsSrF₃.

Table 2. Energy gap at high symmetry points for CsSrF₃.

| Method | Band gap type | Symmetry points | Energy gap (eV) |
|--------|---------------|-----------------------------|-----------------|
| WIEN2K | Direct gap | $\Gamma \rightarrow \Gamma$ | 6.34 |

3.2. Band structure and density of states

The calculated energy bands along the high symmetry lines in the Brillouin zone and total, partial density of states of CsSrF₃ are shown in Figs. 3 and 4 respectively. The zero of energy is chosen to coincide with the valence band maximum (VBM), which occurs at Γ point, and conduction band minimum (CBM) which also occurs at the same Γ point with energy gap 6.34 eV. Thus, CsSrF₃ is a direct and wide band gap insulator. This wide band gap material may be suitable in the applications for the high frequency UV devices. In valence band the bands at -5 eV originate from Cs-5p orbitals, and from -1.8 to 0 eV originate from F-2p orbitals. In the valence band near the Fermi energy, the bands are due to the F-2p, Sr-4p, and small contribution from Cs-5p, Sr-3d, Sr-5s orbitals. In the conduction band, the bands are due to Sr-3d, Cs-4d at the lower part and at the upper part is due to Cs-4f orbitals.

The valence band is composed of majority Cs-5p and F-2p orbitals and conduction band is mainly contributed by Sr-3d and Cs-4f orbitals. The calculated band gap of CsSrF₃ is shown in Table 2.

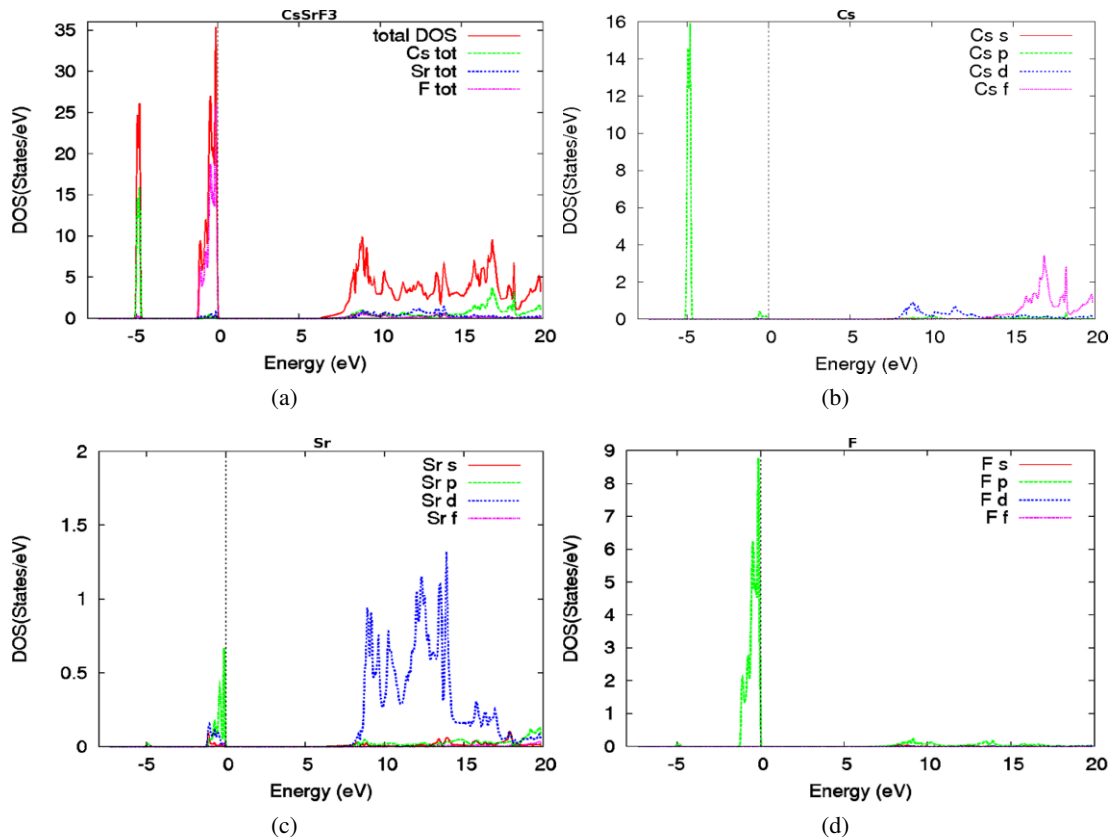


Fig. 4. (a) Total and partial density of states for (b) Cs, (c) Sr and (d) F in CsSrF₃.

The charge density distributions are shown in Fig. 5. Charge density maps serve as a complementary tool for achieving a proper understanding of the electronic structure of the system being studied. The ionic character of any material can be related to the charge transfer between the cation and anion while the covalent character is related to the sharing of the charge among the cation and anion. The covalent behaviour is due to hybridization of Sr-p, Sr-d with the F-p states in the valence band near the Fermi Energy level (Fig. 4). From the figures it is clear that the highest charge density occurs in the immediate vicinity of the nuclei. The near spherical charge distribution around the Cs indicates that the bond between Cs and F is strongly ionic, with no charge sharing among the contours of the respective atoms. It can be seen that most of charge is populated in the Sr-F bond direction, while the maximum charge resides on the Sr and F sites. Hence, a strong

ionic bonding in Cs-F and a mixture of ionic and weak covalent bonding in SrF₂ are observed. The interaction between Cs-Cs may occur because of the significant difference between the large sized Cs⁺ ions and small F⁻ ions (see in Fig. 5(d)). It is interesting to observe that the charge density distribution is in good agreement with the findings of Victor Luana et al. [9]. On comparison we find that the bonds existing between Cs-F and SrF₂ are in good agreement with our work.

3.3. Optical Properties

The FP-LAPW is a good theoretical tool for the calculation of the optical properties of a compound. They give useful information about the internal structure of the CsSrF₃ compound. The dielectric function $\epsilon(\omega) = \epsilon_1(\omega) + i\epsilon_2(\omega)$ is known to describe the optical response of the medium at all photon energies. The imaginary part $\epsilon_2(\omega)$ is directly related to the electronic band structure of a material

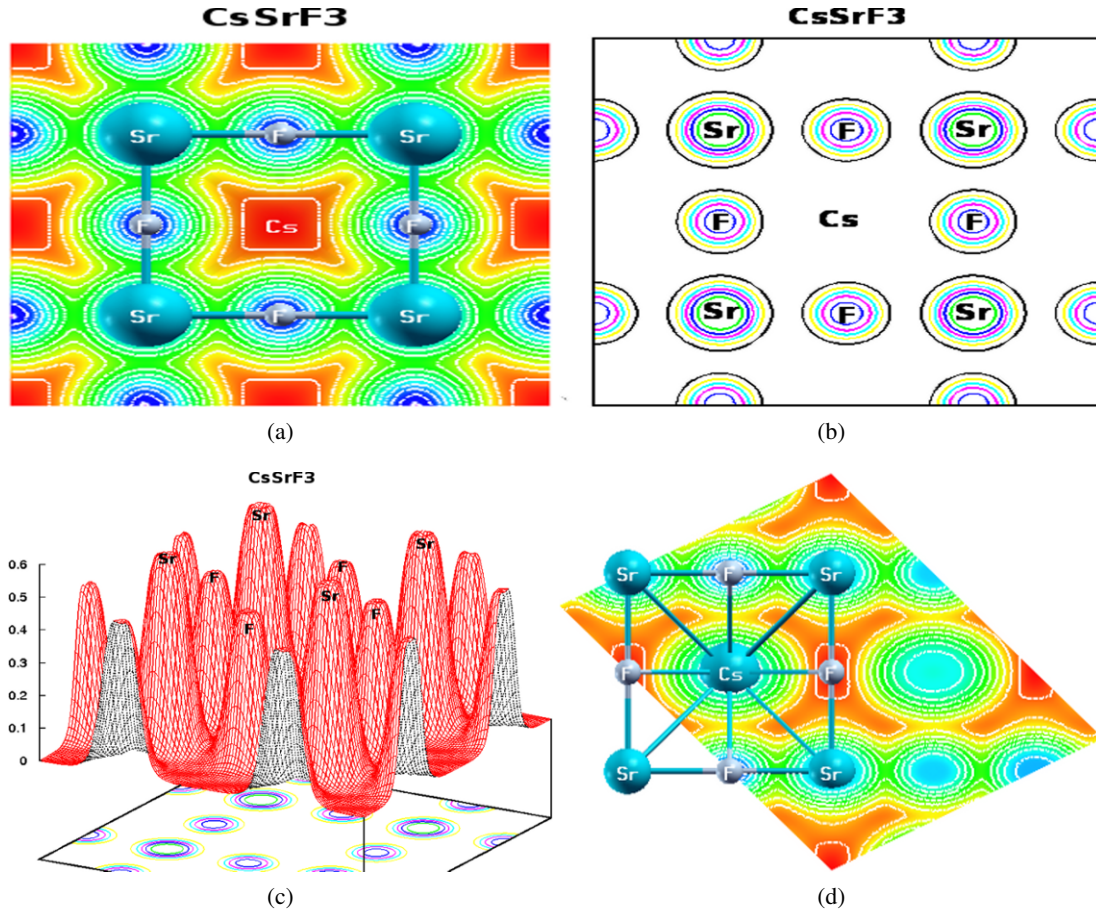


Fig. 5. Charge density distribution of CsSrF₃ (a) along (1 0 0) plane in 2-D representation, (c) along (1 0 0) plane in 3-D representation (d) along $\langle 110 \rangle$ direction.

and describes the absorptive behaviour. In the study of the imaginary part of the dielectric function, $\epsilon_2(\omega)$ is given [24, 25] by:

$$\epsilon_2(\omega) = \left(\frac{4\pi^2 e^2}{m^2 \omega^2} \right) \sum_{i,j} \int_k \langle i | M | j \rangle^2 f_i (1 - f_j) \delta(E_{j,k} - E_{i,k} - \omega) d^3 k \quad (3)$$

where, M is the dipole matrix, i and j are the initial and final states respectively, f_i the Fermi distribution function for the i-th state, and E_i is the energy of electron in the i-th state with the crystal wave vector k. The real part $\epsilon_1(\omega)$ of the dielectric function can be extracted from the imaginary part using the

Kramers-Kronig relation in the form [26, 27]:

$$\epsilon_1(\omega) = 1 + \frac{2}{\pi} P \int_0^\infty \frac{\omega' \epsilon_2(\omega') d\omega'}{\omega'^2 - \omega^2} \quad (4)$$

where, P implies the principal value of the integral. The knowledge of both the real and imaginary parts of the dielectric tensor allows the calculation of important optical functions such as the refractive index $n(\omega)$, extinction coefficient $k(\omega)$ and reflectivity $R(\omega)$, which can be calculated using the following expressions:

$$n(\omega) = \left\{ \frac{\epsilon_1(\omega)}{2} + \frac{\sqrt{\epsilon_1(\omega)^2 + \epsilon_2(\omega)^2}}{2} \right\}^{\frac{1}{2}} \quad (5)$$

$$k(\omega) = \left\{ \frac{\epsilon_1(\omega)}{2} - \frac{\sqrt{\epsilon_1(\omega)^2 + \epsilon_2(\omega)^2}}{2} \right\}^{\frac{1}{2}} \quad (6)$$

$$R(\omega) = \left| \frac{\sqrt{\varepsilon(\omega)} - 1}{\sqrt{\varepsilon(\omega)} + 1} \right|^2 \quad (7)$$

Other optical parameters like energy loss function $L(\omega)$, absorption coefficient $\alpha(\omega)$, and frequency dependent optical conductivity $\sigma(\omega)$ are calculated with the following expressions:

$$L(\omega) = \text{Im} \left(-\frac{1}{\varepsilon(\omega)} \right) \quad (8)$$

$$\alpha(\omega) = \frac{4\pi k(\omega)}{\lambda} \quad (9)$$

$$\sigma(\omega) = \frac{2W_{cv}\hbar\omega}{E_0^2} \quad (10)$$

where, W_{cv} is transition probability per unit time.

The calculated optical properties of CsSrF₃ are shown in Figs. 6 and 7, respectively. The imaginary $\varepsilon_2(\omega)$ and real $\varepsilon_1(\omega)$ parts of the dielectric function are shown in Figs. 6(a) and 6(b), as functions of the photon energy in the range 0-30 eV. In Fig. 6(a), there are mainly 6 peaks observed at 8.95, 13.75, 15.08, 16.35, 21.05 and 24.25 eV. These peaks are identified by the symbols A (8.95), B (13.75), C (15.08), D (16.35), E (21.05) and F (24.25). The threshold energy of the dielectric function occurs at $E_0 = 6.3$ eV, which corresponds to the fundamental gap at equilibrium. It is well known that the materials with band gaps larger than 3.1 eV work well in the ultraviolet region of the spectrum [28, 29]. The peaks A, B, C, and D originate from the electronic transitions from F-2p, Sr-4p in the valence band to the Sr-4d state in the conduction band while the peaks E and F emerge due to the transition from Cs-5p, F-2p, Sr-4p in the valence band to Cs-4d and Cs-4f in the conduction band.

The real part of the dielectric function is displayed in Fig. 6(b). This function $\varepsilon_1(\omega)$ gives us information about the electronic polarizability of a material. The static dielectric constant at zero is obtained as $\varepsilon_1(0) = 2.26$. From its zero

frequency limit, it starts increasing and reaches the maximum value of 3.96 at 8.29 eV. Above 13.15 eV, at 3.15 it starts decreasing and goes below 0 in negative scale for the ranges of 13.92-14.75 eV and 25.47-25.96 eV. At negative values of real dielectric function $\varepsilon_1(\omega)$, this material shows the metallic behaviour otherwise it is dielectric.

The refractive index and the extinction coefficient are displayed in Figs. 6(c) and 6(d) respectively. When we look at the behaviour of imaginary dielectric function $\varepsilon_2(\omega)$ and extinction coefficient $k(\omega)$, a similar trend is observed in Figs. 6(a) and 6(d). Frequency dependent refractive index $n(\omega)$, reflectivity $R(\omega)$, and optical conductivity $\sigma(\omega)$ are also calculated and the salient features of the spectra are presented in Table 3. The static refractive index $n(0)$ is found to have the value of 1.50. The refractive index reaches a maximum value of 2.04 at 8.40 eV. The refractive index is greater than one because as photons enter a material they are slowed down by the interaction with electrons. The more photons are slowed down while travelling through a material, the greater the material's refractive index. Generally, any mechanism that increases electron density in a material also increases refractive index. However, refractive index is also closely related to bonding. In general, ionic compounds have lower values of refractive index than the covalent ones. In covalent bonding more electrons are shared by the ions than in ionic bonding; thus, more electrons are distributed through the structure and interact with the incident photons to slow down.

The optical reflectivity $R(\omega)$ is displayed in Fig. 7(a). The zero-frequency reflectivity is 4.06 %, which remains almost the same upto 6.3 eV. The small value of reflectivity in the infrared and visible energy range shows that the material is transparent in this range. Thus it can be used as an anti-reflecting coating material in this part of the energy spectrum. The maximum reflectivity value is about 29.34 % which occurs at 14.02 eV. Interestingly, the maximum reflectivity occurs where the real part of dielectric function $\varepsilon_1(\omega)$ goes below zero, as seen from Figs. 6(b) and 7(a). The energy loss function is displayed in Fig. 7(b).

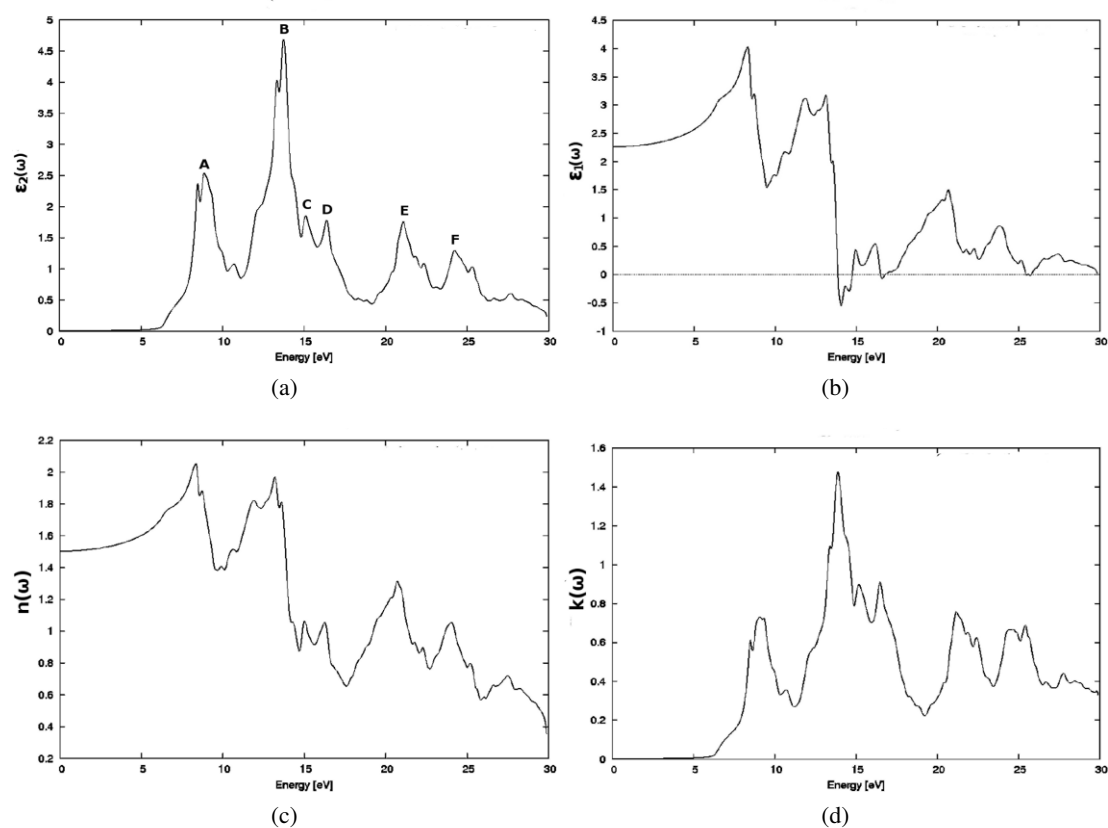


Fig. 6. Optical spectra as a function of photon energy for cubic perovskite CsSrF₃ (a) imaginary, (b) real parts of dielectric function, (c) refractive index and (d) extinction coefficient of CsSrF₃.

Table 3. Calculated zero frequency limits of refractive index $n(0)$, reflectivity $R(0)$, energy range for $n(\omega) < 1$, maximum value of refractive index $n(\omega)$, reflectivity $R(\omega)$ and optical conductivity $\sigma(\omega)$ of CsSrF₃.

| CsSrF ₃ | $n(0)$ | Maximum $n(\omega)$ | Energy range (in eV) for $n(\omega) < 1$ | $R(0)$ % | Maximum $R(\omega)$ | Maximum $\sigma(\omega)$ (in $\Omega^{-1} \text{cm}^{-1}$) |
|--------------------|--------|---------------------|---|----------|---------------------|---|
| This work | 1.50 | 2.04 | 14.42-14.86 15.14-16.02 16.41-19.28 21.43-23.70 24.25-30.00 | 4.06 | 29.34 | 8577.27 |

The energy loss function $L(\omega)$ is an important factor describing the energy loss of a fast electron traversing in a material. The peaks in $L(\omega)$ spectra represent the characteristics associated with the plasma resonance. The resonant energy loss is seen at 30 eV. The optical conductivity $\sigma(\omega)$ is shown in Fig. 7(c). It starts from 6.34 eV and the maximum value of optical conductivity of the compound is obtained at 13.74 eV with a magnitude

of $8577.27 \Omega^{-1} \text{cm}^{-1}$. Similar features are also observed in absorption coefficient $\alpha(\omega)$, in the absorption range upto 30 eV and it is shown in Fig. 7(d). CsSrF₃ is the direct band gap compound and has high absorption power in the visible and ultraviolet energy range, so it can be used in the optoelectronic devices such as UV detectors, and can also be used in anti-reflection coatings. CsSrF₃ is the cubic perovskite fluoride with a wide band

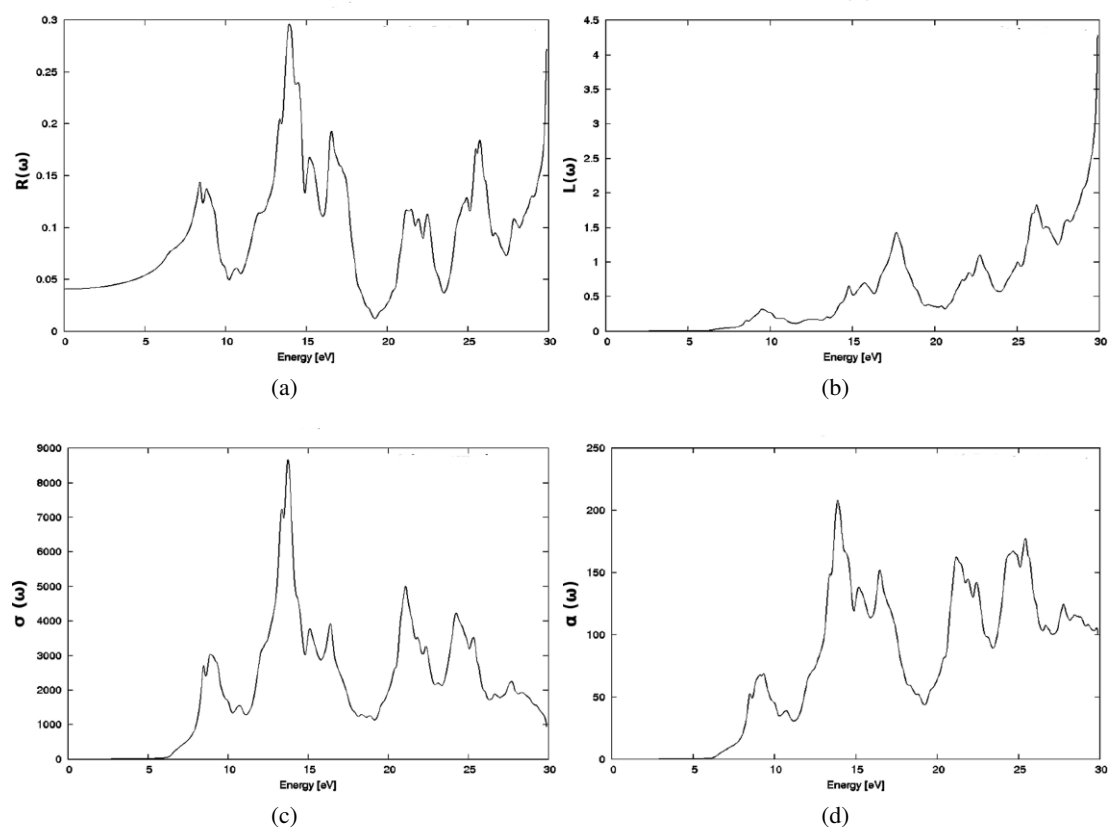


Fig. 7. Optical spectra as a function of photon energy for cubic perovskite CsSrF_3 (a) reflectivity, (b) energy loss function, (c) optical conductivity, (d) absorption coefficient.

gap, which is useful as the vacuum-ultraviolet transparent (VUV-transparent) material for lens in optical lithographic technology [30].

4. Conclusions

In this paper, we have studied the electronic, structural and optical properties of the cubic perovskite CsSrF_3 using the FP-LAPW + local orbitals method within the generalized gradient approximation (GGA) in the framework of density functional theory. The lattice constant is found to be in good agreement with the experimental result. It is found that the compound has a wide and direct band gap of 6.34 eV. The compound has strong ionic bonding in CsF , and a mixture of ionic and weak covalent bonding in SrF_2 . The optical properties such as dielectric function, reflectivity, absorption coefficient, real part of optical conductivity, refractive index, extinction

coefficient and electron energy loss were studied in the energy range of 0–30 eV. The material has direct band gap and small value of reflectivity, which suggests that it is useful in anti-reflection coatings, and optoelectronic devices.

References

- [1] R. EL OUEZERFI et al., *J. Appl. Phys.*, 96 (2004), 7655.
- [2] SHIMAMURA K. et al., *Cryst. Res. Technol.*, 36 (2001), 801.
- [3] SETTER N. et al., *J. Appl. Phys.*, 100 (2006), 051606.
- [4] ZHANG F., MAO Y., PART T.-J., WONG S. S., *Adv. Funct. Mater.*, 18 (2008), 103.
- [5] LIM S.H., RASTOGI A. C., DESU S. B., *J. Appl. Phys.*, 96 (2004), 5673.
- [6] VERMA A.S., JINDAL V.K., *J. Alloys Compd.*, 485 (2009), 514.
- [7] SPRINGIS M., SHARAKOVSKY A., TALE I., ROGULIS U., *Phys. Stat. Sol. (c)* 2 (2005), 511.
- [8] HU Y .X., WU S. Y., WANG X. F., LI L .L., *J. Phys.*, 72 (2009), 989.
- [9] LUANA V., COSTALES A., PENDAS A. M., *Phys. Rev.*

- B*, 55 (1997), 4285.
- [10] MURTAZA G., MAQBOOL M., RAHNAMEYE ALIABAD H. A., AFAQ A., *Chin. Phys. Lett.*, 28 (2011), 117803.
- [11] MARVIN J. Weber., Handbook of Optical Materials., 1932.
- [12] VOPILOV E. A., VORONOV V. N., BUZNIK V. M., *J. Stru. Chem.*, 20 (1979), 638.
- [13] JIANGA L. et al., *J. Phys. Chem. Solids*, 67 (2006), 1531.
- [14] DANTAS J. M., LALIC M. V., *Optical Materials*, 32 (2010), 1633.
- [15] MURTAZA G., IFTIKHAR AHMAD., AMIN B., AFAQ A., MAQBOOL M., *Optical Materials*, 33 (2011), 553.
- [16] MURTAZA G., SADIQUE G., RAHNAMEYE ALIABAD H. A., KHALID M. N., NAEEM S., *Physica B*, 406 (2011), 4584.
- [17] PERDEW J. P. et al., *Phys. Rev. B*, 46 (1992), 6671.
- [18] PERDEW J. P., *Physica B*, 172 (1991), 1.
- [19] GOUDOCHNIKOV P., BELL A.J., *J. Phys. Condens. Matter*, 19 (2007), 176201.
- [20] LI C., WANG B., WANG R., WANG H., LU X., *Physica B*, 403 (2008), 539.
- [21] BLAHA P., SCHWARZ K., MADSEN G. K. H., KVASNICKA D., LUITZ J., in WIEN 2K: An Augmented Plane Wave Plus Local Orbitals Program for Calculating Crystal Properties, Ed. by K. Schwarz (Vienna Technological University, Vienna, Austria, 2001).
- [22] PERDEW J. P., BURKE S., ERNZERHOF M., *Phys. Rev. Lett.* 77 (1996), 3865.
- [23] MURNAGHAN F. D., *Proc. Natl. Acad. Sci. USA*, 30 (1944), 244.
- [24] SMITH N.V., *Phys. Rev. B*, 3 (1971), 1862.
- [25] AMBROSCH-DRAXL C., SOFO J.O., *Comput. Phys. Commun.*, 175(2006), 1.
- [26] FOX M., Optical Properties of Solids, Oxford University Press, New York, 2001.
- [27] WOOTEN F., Optical properties of Solids, Academic Press, New York, 1972, p.179.
- [28] MAQBOOL M., AMIN B., AHMED I., *J. Opt. Soc. Am., B*, 26 (2009), 2180.
- [29] MAQBOOL M., KORDESCH M. E., KAYANI A., *J. Opt. Soc. Am. B*, 26 (2009), 998.
- [30] SAHNOUN M., ZBIRI M., DAUL C., KHENATA R., BALTACHE H., DRIZ M., *Materials Chemistry and Physics.*, 91 (2005), 185.

Received 2012-03-20

Accepted 2012-09-1